ORIGINAL PAPER

Insights into interstitial flow, shear stress, and mass transport effects on ECM heterogeneity in bioreactor-cultivated engineered cartilage hydrogels

Tony Chen · Mark Buckley · Itai Cohen · Lawrence Bonassar · Hani A. Awad

Abstract Interstitial flow in articular cartilage is secondary to compressive and shear deformations during joint motion and has been linked with the well-characterized heterogeneity in structure and composition of its extracellular matrix. In this study, we investigated the effects of introducing gradients of interstitial flow on the evolution of compositional heterogeneity in engineered cartilage. Using a parallel-plate bioreactor, we observed that Poiseuille flow stimulation of chondrocyte-seeded agarose hydrogels led to an increase in glycosaminoglycan and type II collagen deposition in the surface region of the hydrogel exposed to flow. Experimental measurements of the interstitial flow fields based on the fluorescence recovery after photobleaching technique suggested that the observed heterogeneity in composition is associated with gradients in interstitial flow in a boundary layer at the hydrogel surface. Interestingly, the interstitial flow velocity profiles were nonlinearly influenced by flow rate, which upon closer examination led us to the original observation that the apparent hydrogel permeability decreased exponentially with increased interfacial shear stress. We also observed that interstitial flow enhances convective mass transport irrespective of molecular size within the boundary layer near the hydrogel surface and that the convective contribution to transport diminishes with depth in association with interstitial flow gradients. The implications of the nonlinearly inverse relationship between the interfacial shear stress and the interstitial flux and permeability and its consequences for convective transport are important for tissue engineering, since porous scaffolds comprise networks of Poiseuille channels (pores) through which interstitial flow must navigate under mechanical stimulation or direct perfusion.

T. Chen · H. A. Awad
Department of Biomedical Engineering, University of Rochester, Rochester, NY, USA

T. Chen · H. A. Awad (✉)
Department of Biomedical Engineering,
The Center for Musculoskeletal Research,
University of Rochester Medical Center,
Box 665, 601 Elmwood Avenue,
Rochester, NY 14642, USA
e-mail: hani_awad@urmc.rochester.edu

M. Buckley · I. Cohen
Department of Physics, Cornell University, Ithaca, NY, USA

L. Bonassar
Department of Biomedical Engineering, Cornell University, Ithaca, NY, USA

1 Introduction

Articular cartilage is characterized by anisotropy in composition and architecture that affects its biomechanics and mechanobiology. This anisotropy plays important roles in supporting "physiologic" loading and facilitating the nearly frictionless articular motion throughout the healthy life of the joint (Carter et al. 2004; Carter and Wong 2003; Lammi 2004; Wong and Carter 2003). Physiologic loading affects the chondrocytes' metabolic activity and cartilage composition, structure, and function through several mechano-electrochemical transduction mediators including compressive, shear, and tensile strains, hydrostatic pressure, interstitial fluid flow, streaming potentials, and convective molecular transport

(Gray et al. 1988). Therefore, the intimate coupling between composition, structure, and biomechanical function has important implications in functional tissue engineering of cartilage (Butler et al. 2000).

Functional tissue engineering is a scientific paradigm that addresses the influence of biomechanical and physical factors in bioreactor systems on the differentiation and metabolic activity of cells and engineered tissues and organs. Early generations of cartilage bioreactors were designed to overcome diffusion limitation in clinical scale constructs, by improving mixing of media and convective transport through various hydrodynamic designs (Freed et al. 1998, 1993). Others have demonstrated that applying dynamic compressive deformations that mimic in vivo joint loads stimulate the biosynthetic activity of chondrocytes in cartilage explants (Bonassar et al. 2001; Sah et al. 1989) and recognized that this can be replicated in tissue engineering bioreactors (Buschmann et al. 1995; Mauck et al. 2000) to improve the biochemical composition and biomechanical properties of tissue engineered cartilage constructs (e.g. agarose hydrogels) over time (Hung et al. 2004). Interestingly, in this unconfined compression setup, the observed enhancement in chondrocyte biosynthetic activity has been co-localized with increased interstitial fluid flow on the periphery of the constructs and did not seem to be locally associated with fluid pressure or compressive strains in these peripheral regions, suggesting an important mechanotransduction role for interstitial fluid flow (Buschmann et al. 1995, 1999). While the mechanism of flow-induced mechanotransduction may vary in different cell types, as it has been reported to involve integrin-mediated and stretch-activated ion channel signaling in chondrocytes (Lee et al. 2000), heparin-sulfate-mediated FAK signaling in smooth muscle cells (Shi et al. 2011), and primary cilia-mediated signaling in bone cells (Malone et al. 2007), it is widely recognized that the flow-related mechanobiology has important implications in cell differentiation, tissue morphogenesis, and tissue engineering. In addition to its mechanotransduction role, it has also been long recognized that interstitial flow leads to compaction of the extracellular matrix and consequently to heterogeneity in the structure and composition of the extracellular matrix (Mow and Wang 1999). Furthermore, interstitial flow has been shown to create gradients of soluble signals, which could alter cell behavior such as migration, as has been demonstrated in the tumor microenvironment (Shieh and Swartz 2011). Consistent with these observation, perfusion bioreactors that induce interstitial fluid flow through tissue engineered constructs have been shown to increase chondrogenic matrix production in engineered cartilage in the absence of compressive strains, presumably through convective transport and shear stress stimulation of the cells (Bujia et al. 1995; Pazzano et al. 2000; Sittinger et al. 1994). Despite the reported beneficial effects of bioreactor culture on the composition and bio-

mechanical integrity of engineered cartilage, reproducing the native tissue's heterogeneous zonal organization and the associated functional anisotropy in engineered cartilage constructs remains an unsolved challenge for tissue engineers.

To address this challenge, we previously reported using computational fluid dynamics (CFD) modeling that Poiseuille flow over a hydrogel construct induces depth-dependent gradients in interstitial fluid flow velocity in agreement with theory (Beavers and Joseph 1967; Hou et al. 1989), and we hypothesized that this flow would induce compositional heterogeneity and differentially affect collagen alignment (Lamkin-Kennard et al. 2005). Gemmiti and Guldberg (2006) experimentally demonstrated that Poiseuille flow-induced shear stress magnitude and duration in a parallel-plate bioreactor modulate a heterogenous matrix composition, and differentially align the collagen fibers in the extracellular matrix in engineered cartilaginous tissue, thereby influencing its tensile mechanical properties (Gemmiti and Guldberg 2006, 2009). In subsequent work, Pierre et al. (2008) demonstrated, using finite element modeling, that the shear stress could modulate the level and distribution of tissue oxygenation (Pierre et al. 2008). However, whether the reported flow effects on the compositional and structural inhomogeneity are due to interstitial flow and shear stress stimulation or convective transport of nutrients such as glucose and various growth factors remains to be determined. To address this question, an accurate mapping of the interstitial flow fields and mass transport within the engineered cartilage constructs needs to be determined to help model the hydrodynamics and mass transport effects. To that end, this study was designed to microscopically characterize the interstitial flow fields and their effects on convective transport within agarose hydrogels in a Poiseuille flow parallel-plate bioreactor system. We first evaluated the effects of Poiseuille flow stimulation on matrix composition in chondrocyte-seeded agarose hydrogels. We then used a flow visualization technique based on the Fluorescent Recovery After Photobleaching (FRAP) method to measure the interstitial fluid flow velocity and evaluate its effects on mass transport at different depths within the agarose hydorgel. The nonlinear coupling between the flow rate, shear stress, apparent permeability, and mass transport was evaluated through a combination of theoretical considerations of interstitial flow in biphasic mixtures under Poiseuille flow (Hou et al. 1989) and Computational Fluid Dynamics (CFD) modeling.

2 Methods

2.1 Bioreactor design

The parallel-plate bioreactor used in chondrocyte-seeded hydrogel experiments consists of three main compartments
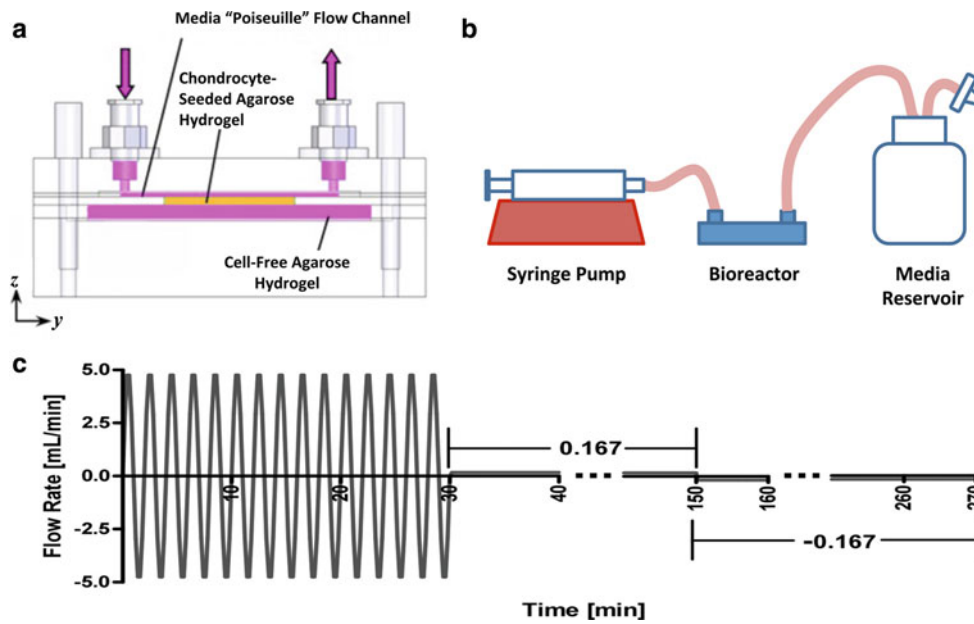
Fig. 1 A 2D schematic of the Poiseuille flow bioreactor showing: **a** The upper rectangular flow channel through which media is perfused with a pump, the rectangular cavity to hold the tissue engineered cartilage (TEC) hydrogel (2% agarose seeded with 40 million chondrocytes/ml), and the bottom compartment containing an acellular hydrogel to maintain the TEC hydration. **b** The experimental setup in which a syringe pump drives flow in the parallel-plate bioreactor in a cyclic fashion (1 Hz) at ± 5 ml/min estimated to induce a nominal shear stress of ± 0.012 Pa at the interface between the culture medium in the flow channel and the surface of the TEC hydrogel. The flow regimen is repeated over 7 days following an initial static culture period of 14 days

(Fig. 1a). The upper compartment comprises a rectangular flow channel (1.25 mm height) with inlet and outlet ports that connect via silastic tubing to a programmable syringe pump (New Era Pump Systems Inc, Wantagh NY) and a culture media reservoir, respectively (Fig. 1b). The middle compartment comprises a rectangular cavity (2 mm deep) into which the chondrocyte-seeded 2% agarose (tissue engineered cartilage or TEC) hydrogel is cast. A cell-free 1.25% agarose hydrogel is cast within the bottom compartment (4 mm deep) to provide hydration to the bottom of the TEC hydrogel and anchor it in place.

The nominal shear stress across the surface of the TEC hydrogel is approximated by

$$\tau = \frac{6\mu Q}{bh^2} \tag{1}$$

where τ is the shear stress, μ is the dynamic viscosity, Q is the flow rate, and b and h are the width and height of the flow channel, respectively. Based on the dimensions of the chambers (Table 1), a flow rate (Q) of 5 ml/min results in a nominal shear stress of 0.012 Pa across the surface of the TEC hydrogel.

2.2 Chondrocyte isolation and tissue engineered cartilage (TEC) hydrogels

All reagents were purchased from Invitrogen (Carlsbad, CA) unless otherwise noted. Chondrocytes were isolated from the elbow joints of pigs within 24 h after slaughter. The joint space was opened using aseptic technique; cartilage bits were shaved from the articulating ends of the ulna, radius, and humerus of the elbow joint and placed into wash media consisting of DMEM (high glucose), 20% Fetal Bovine Serum (FBS), 1% Penicillin/Streptomycin (P/S), Kanamycin Sulfate (Sigma-Aldrich, St. Louis MO), and Fungizone and Gentamicin. The cartilage was then minced into finer (2 mm × 2 mm) pieces and enzymatically digested using pronase (Cal-BioChem, San Diego CA) for 1.5 h followed by type-2 collagenase (Worthington Biochemical, Lakewood NJ) for 16 h. The digested tissue suspension was then strained through a 40 μm cell strainer, and the retrieved cells were washed twice and then suspended in complete media (DMEM/F-12, 10% FBS, 1% P/S) until used to create the TEC hydrogels.

Isolated cells were suspended in complete media and mixed with molten ($\sim 40°C$) type VII agarose (Sigma-Aldrich) in PBS to create a 40×10^6 cells/ml 2% agarose solution. The chondrocyte/agarose solution was cast in the hydrogel cavity of the middle bioreactor compartment and allowed to polymerize at room temperature for 20 min to form the TEC hydrogel. Following 14 days of preculture in an incubator, the bioreactor containing the TEC hydrogel was assembled, placed in an incubator at 37°C and 5% CO_2, and connected to the syringe pump and media reservoir using flexible tubing. Since intermittent loading has been shown to induce anabolic effects in chondrocyte-seeded agarose hydrogels (Mauck et al. 2003),

Table 1 Bioreactor design and operational parameters

		Large cell culture bioreactor	Scaled-down FRAP bioreactor
Nominal bioreactor dimensions			
Media flow channel			
	Height (h_1)	1.25 mm	0.2 mm
	Width (w_1)	18 mm	20 mm
	Length (L_1)	50 mm	46 mm
TE hydrogel (2% agarose) compartment			
	Height (h_2)	2 mm	0.32 mm
	Width (w_2)	15 mm	2.4 mm
	Length (L_2)	30 mm	4.8 mm
Bottom hydration (1.25% agarose) compartment			
	Height (h_3)	4 mm	0.64 mm
	Width (w_3)	20 mm	3.2 mm
	Length (L_3)	65 mm	10.4 mm
Flow media properties			
Media density	ρ	1,000 kg/m^3	
Media viscosity	μ	6.9×10^{-4} Ns/m^2	
Media flow rate	Q	Oscillatory (1 Hz) flow ± 5 ml/min*	Steady flow 0.014–0.14 ml/min
		Resting (steady) flow $\sim$0.167 ml/min*	
Nominal interfacial shear stress	$\tau_{hs} = 6\mu Q/w_1 h_1^2$	Oscillatory (1 Hz) flow ± 0.012 Pa	0.0012–0.012 Pa
		Resting (steady) flow $\sim$ 0.0004 Pa	
TE hydrogel properties			
Chondrocytes number density		40×10^6 cells/ml	N/A
Fluid volume fraction	ϕ^f	0.98	

* See Fig. 1 for flow regimen

the syringe pump, controlled externally via custom-written Labview (National Instruments, Austin TX) software, was programmed to perfuse culture media at ± 5 ml/min in a full 1 Hz sinusoidal wave for 30 min once daily, followed by steady flow at 0.167 ml/min for the remainder of the day (alternating steady-state infusion and withdrawal every 2 h) (Fig. 1c). This regimen was repeated over for 7 days. Control TEC hydrogels were created similarly and cultured in a petri dish in the incubator at 37°C for 21 days. In both the control and the bioreactor-cultivated hydrogels, the media was supplemented with 189 mM fresh ascorbate every 3 days. At the end of 21 days, specimens (5 mm diameter) were collected from the control and bioreactor-cultivated TEC hydrogels and used for biochemistry and histology.

2.3 Biochemical and histological analyses

For biochemical analyses, specimens were digested using 0.5 Units/ml of papain (Sigma-Aldrich) with 2 mM L-cysteine (Sigma-Aldrich) and 2 mM ethylenediaminetetraacetic acid (EDTA; Sigma-Aldrich) for 16 h. The dissolved specimens were stored frozen at -80°C until assayed using Hydroxyproline, Dimethylmethylene Blue (DMMB), and Picogreen assays for collagen, sulfated-glycosaminoglycan (s-GAG), and DNA content, respectively (Awad et al. 2004).

For histology, specimens were fixed in 10% Neutral Buffered Formalin (NBF) at room temperature for 24 h. Samples were then removed from the NBF and dehydrated under vacuum through graded alcohol steps (30, 50, 70, 80, 95 and 100% ethanol) for 1 h each, followed by two 15 min washes in Xylenes (Sigma-Aldrich, St. Louis MO). Samples were then infiltrated with paraffin at 60°C for 2 h under vacuum before embedding. After sections were embedded in paraffin, 5 μm sections were cut and stained with Toluidine Blue or processed for immunohistochemistry. Briefly, sections were quenched of endogenous peroxidases using 3% hydrogen peroxide (MediChoice, Mechanicsville VA). Sections were then blocked for an hour with a 2% solution of Normal Horse Serum (Vector Labs, Burlingame CA) followed by a 1:100 dilution of mouse anti-Collagen II (II-II6B3; Developmental Studies Hybridoma Bank, The University of Iowa) in Normal Horse Serum. Biotinylated horse anti-mouse secondary antibody (Vector Labs) was added for 30 min followed by addition of HRP (Thermo Scientific, Rockford IL) for 20 min.
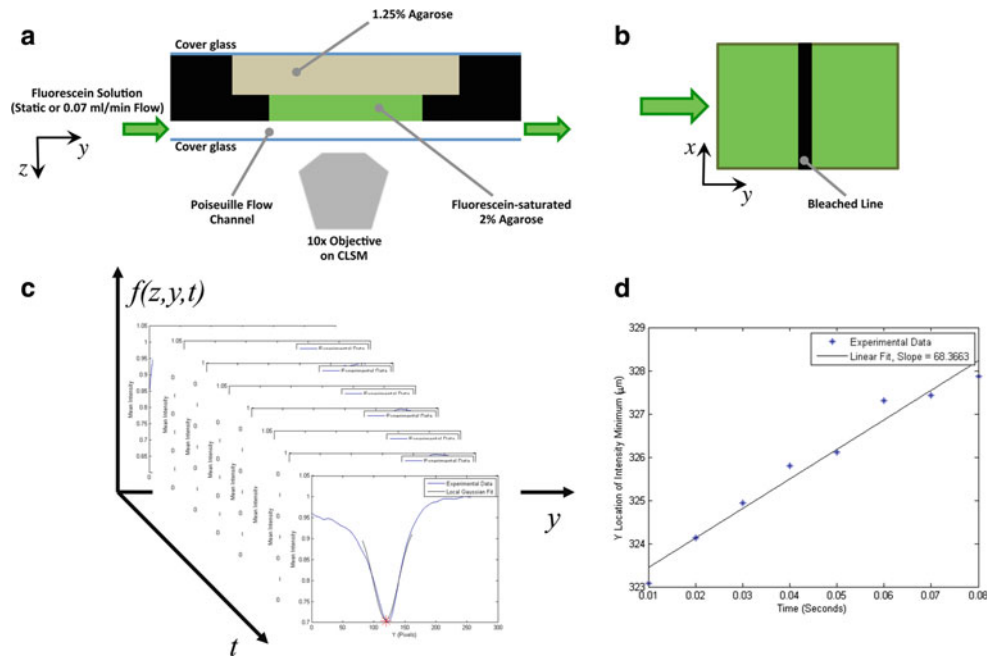
Fig. 2 A 2D Schematic of the fluorescence recovery after photobleaching (FRAP) experimental setup to measure the fluid flow velocity in the flow channel and within the TEC hydrogel. **a** A scaled-down replica of the Poiseuille flow bioreactor is used to measure flow velocity on a laser scanning confocal microscope using FRAP. **b** After soaking the TEC hydrogel (acellular 2% agarose) in Sodium Fluorescein (0.125 mg/ml) for 24 h, a 12.4-micron thick line is photobleached. A Fluorescein solution is then pumped in the Poiseuille flow channel at flow rates from 0.014 to 0.14 ml/hr to induce nominal interface shear stresses of 0.0012– 0.012 Pa. The intensity of the fluorescence in the field of view is measured from sequential images recorded over time and normalized by the average intensity prior to bleaching and fitted to Green's function solution that accounts for diffusive and convective recovery of the fluorescence (**c**). The flow velocity is then determined linear regression of the y (flow direction coordinate) locations of the fluorescence Gaussian minima with time (**d**). The measurements were repeated at various depths at 10-micron intervals in the flow channel and the TEC hydrogel compartment

Romulin AEC Chromogen (Biocare Medical, Concord CA) was used to detect conjugated antibodies.

2.4 Interstitial flow and mass transport measurements

To facilitate confocal microscopy imaging of the fluorescent tracers used for visualization of the flow and mass transport in the channel and interstitially in the hydrogel, a proportionally scaled-down prototype of the parallel-plate bioreactor was designed with dimensions that allow imaging through a glass coverslip, the flow channel (200 μm), and up to 100 μm deep into the 2% agarose hydrogel. The dimensions of the scaled prototype and the flow regimen (Table 1) were designed to generate nominal shear stresses ranging from 0.0012 to 0.012 Pa across the surface of the hydrogel, to encompass the surface shear stress experienced by the chondrocyte-seeded TEC hydrogels.

A flow visualization technique based on fluorescence recovery after photobleaching (FRAP) was used to measure the interstitial fluid velocity within the bioreactor. Agarose hydrogels (2%) were cast within the TE hydrogel compartment of the scaled-down bioreactor and allowed 20 min at room temperature to polymerize. The hydrogel slabs were then removed from the compartment and bathed in a 125 mg/ml aqueous solution of Sodium Fluorescein (Sigma-Aldrich, St. Louis, MO) overnight. The following day, the hydrogels were placed back in their bioreactor compartment, and an anchoring 1.25% agarose hydrogel was cast into the bottom hydrogel compartment and sealed by a glass coverslip. The assembly of the bioreactor was completed by a second coverglass, which created a flow channel over the free surface of the Fluorescein-saturated hydrogel slab. The bioreactor assembly was mounted on the stage of a Zeiss LSM 5 Live confocal microscope (Carl Zeiss, Inc., Thornwood, NY), as depicted in Fig. 2a. The bioreactor was then connected to a syringe pump and a reservoir perfusing an aqueous solution of Sodium Fluorescein at rates ranging from 0.014 to 0.14 ml/min. This range of flow rates was selected to encompass surface shear stresses ranging from 0.0012 to 0.012 Pa, which were selected based on previous reports (Gemmiti and Guldberg 2009) demonstrating shear stress-dependent matrix production in chondrocytes at shear stresses ranging from 0.001 to 0.1 Pa. However, due to limitations in our imaging setup, we were unable to reliably measure fluid velocities at shear stresses greater than 0.012 Pa. Therefore, we used the range of shear stresses from 0.0012 to 0.012 Pa.

The confocal microscope was configured to capture images at a rate of 100 frames per second. Starting approximately at the surface of the hydrogel, twenty frames were captured before a 12.4 µm thick line was photobleached in the center of the imaging frame, after which another 80 frames were captured for imaging and analysis of FRAP (Fig. 2b). Three images were captured at each depth within the hydrogel up to a depth of 100 µm at 10 µm intervals. Similarly, sequences of FRAP images were also taken through the flow channel ($\sim$200 µm) at 10 µm intervals. This process was repeated for each of the flow rates in three independent experiments. The image sequences were exported as AVI movie files using LSM explorer software (Carl Zeiss, Inc) for analysis.

Fluorescence recovery after photobleaching under uniaxial flow can be modeled by the one-dimensional diffusion equation with a uniaxial drift term $v\partial C(y,t)/\partial y$ and an additional term $\rho(y,t)$ representing the production of photobleached molecules by the line-scanning laser. Taking Q_0 to be the laser's bleaching power (Leddy et al. 2006) and assuming that photobleaching occurs at a single instant ($t = 0$) and location ($y = 0$), $\rho(y,t)$ can be written as $Q_0\delta(y)\delta(t)$. Therefore, the experiment can be modeled using the following partial differential equation (PDE):

$$\frac{\partial C(y,t)}{\partial t} = D\frac{\partial C^2(y,t)}{\partial y} - v\frac{\partial C(y,t)}{\partial y} + Q_0\delta(y)\delta(t) \quad (2)$$

where $C(y,t)$ is the concentration of photobleached fluorophores at location y and time t, v is the flow velocity in the y direction, and D is the diffusion constant for the photobleached molecules. This PDE is solved by employing the substitution (Polianin 2002)

$$C(y,t) = \exp(\beta t + \mu y)u(y,t) \quad (3)$$

where $\beta = -\frac{v^2}{4D}$ and $\mu = \frac{v}{2D}$, yielding

$$\frac{du}{dt} = D\frac{d^2u}{dt^2} + \exp\left(-\beta t - \mu y\right)Q_0\delta(y)\delta(t) \quad (4)$$

with the initial condition $C(y,0) = 0$ or $u(y,0) = 0$.

Equation (4) is the nonhomogeneous heat equation, whose solution is given by the integral (Polianin 2002)

$$u = \int\limits_{0}^{t}\int\limits_{-\infty}^{\infty} Q_0\delta(\tau)\delta(y)\exp(-\beta\tau - \mu q)$$
$$G(y,q,t-\tau)dq\,d\tau \quad (5)$$

where $G(y,q,t) = \frac{1}{2\sqrt{\pi Dt}}\exp\left(-\frac{(y-q)^2}{4Dt}\right)$.

Integrating Eq. (4) and solving for $C(y,t)$ yield

$$C(y,t) = \frac{Q_0}{2\sqrt{\pi Dt}}\exp\left(-\frac{(y-vt)^2}{4Dt}\right) \quad (6)$$

Since regions with high concentrations $C(y,t)$ of photobleached molecules appear brightest, the fluorescence intensity profile of the collected images may be written as

$$I(y,t) \propto -\frac{1}{2\sqrt{\pi Dt}}\exp\left(-\frac{(y-vt)^2}{4Dt}\right) \quad (7)$$

The acquired image sequences were analyzed using a custom Matlab (Mathworks, Natick MA) algorithm to track the bleached region in sequential images recorded over time by fitting the fluorescence intensity profile to Eq. (6) (Fig. 2c). This equation describes a Gaussian curve whose width and height increase and decrease in time, respectively, while the global minimum translates in the y-direction with velocity v. Therefore, the flow velocity at each depth was determined from the slope of the plot of the y-coordinate of the minima of the fluorescence intensity versus time (Fig. 2d).

The experimental velocity measurements were fit using a nonlinear least squares analysis to a theoretical biphasic solution of an idealized form of this problem, which was previously described by Hou et al. (1989) based on the classical Beavers-Joseph problem of viscous flow over a rigid porous-permeable medium such as a hydrogel (Beavers and Joseph 1967). This solution predicts that the interstitial flow is enhanced in a boundary layer beneath the hydrogel surface and is influenced by the solid/fluid volume fraction, drag coefficient, the apparent viscosity of the fluid in the hydrogel, and characteristic lengths defining the height and thickness of the flow channel and hydrogel, respectively. The curve fit allows us to eliminate experimental uncertainty in determining the z-coordinate of the interface between the flow channel and the TEC hydrogel (Sect. 1, Supplemental Data).

To investigate Poiseuille-driven interstitial flow effects on mass transport, FRAP-based measurements under flow (0.07 ml/min) or no flow were repeated for different depths within 2% agarose hydrogel slabs saturated in aqueous solutions of various molecular weight FITC- dextran (4, 10, 40, and 70 kDa). The mean fluorescence intensity within the bleached region (normalized to the background intensity prior to photobleaching) was calculated for each image taken at various depths within the hydrogel over the recovery period (0.8 s) and plotted versus time for the various molecular sizes. The recovery of fluorescence within the bleach region over time was used to characterize changes in dye transport. The area under the normalized fluorescence recovery curve was computed to compare the rates of recovery as a function of hydrogel depth and molecular size. Duplicate measurements were performed in
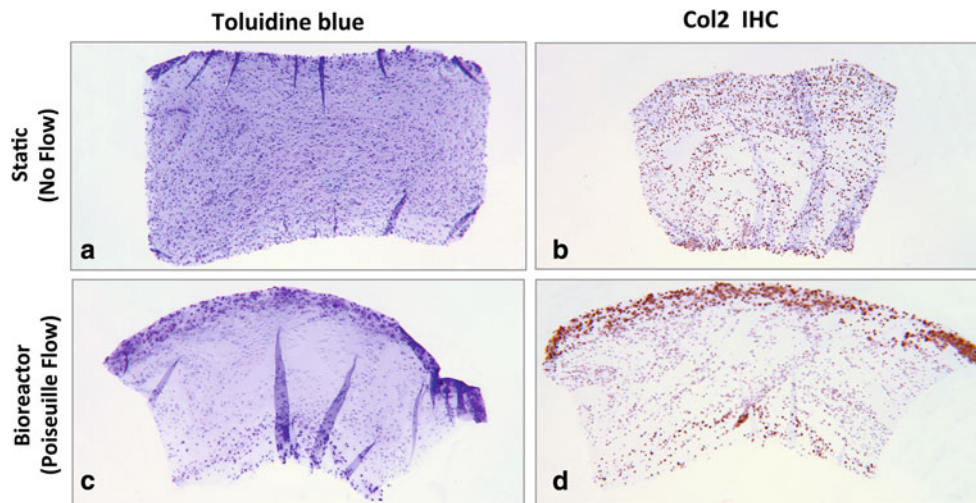
Toluidine blue   **Col2 IHC**

Fig. 3 Effects of the bioreactor cultivation and induced interstitial flow on aggrecan and type II collagen accumulation in the chondrocyte-seeded TEC hydrogel. The constructs were cultured in static (no-flow) conditions for 14 days followed by 7 days of no flow (**a, b**) or under Poiseuille flow stimulation in the bioreactor, in which they were subjected to oscillatory flow ± 5 ml/min in a full 1 Hz sinusoidal wave for 30 min once daily, followed by steady flow at ± 0.167 ml/min for the remainder of the day (alternating steady-state infusion and withdrawal every 2 h) (**c, d**). Note the depth-dependent heterogeneity in composition and collagen alignment in the constructs subjected to Poiseuille flow

3 Results

3.1 Poiseuille flow induces spatial heterogeneity in the ECM distribution of s-GAG and collagen

Biochemical analysis of the extracellular cellular matrix (ECM) demonstrated that Poiseuille flow in the bioreactor did not affect the total s-GAG or collagen content in the chondrocyte/agarose hydrogel ($38.56 \pm 4.61 \mu$g s-GAG/μgDNA vs. $46.67 \pm 14.27 \mu$g s-GAG/μgDNA and $6.18 \pm 4.84 \mu$g collagen/μg DNA vs. $7.07 \pm 1.86 \mu$g collagen/μg DNA, in the bioreactor-cultivated and control specimens respectively, mean $\pm$ standard deviation, $n = 3$). However, while histological sections of control TEC hydrogel samples showed uniform staining for Toluidine Blue and type II collagen, sections sampled from the bioreactor-cultivated TEC hydrogels were consistently characterized by the presence of a ~ 0.24-mm thick layer (about 13% of construct thickness) that stained intensely for Toluidine Blue and type II collagen near the top surface of the construct, which reflects the enhanced metabolic activity of the cells exposed to Poiseuille flow (Fig. 3a–d). It is also worth noting that the cells in the center of the flow-exposed constructs appear to have migrated toward the surface exposed to flow, presumably under the influence of gradients of soluble factors created by the interstitial flow boundary layer, as has been described (Rutkowski and Swartz 2007).

3.2 Interstitial flow gradients and hydrogel permeability are nonlinearly influenced by flow rate

To formally test the hypothesis that the bioreactor induced heterogeneity in s-GAG and type II collagen distribution is associated with interstitial flow fields, the flow velocity profiles within the flow chamber and the TEC hydrogels were experimentally measured as a function of flow rate through a scaled-down parallel-plate (Poiseuille flow) bioreactor and fitted to the Hou and Mow equation of Poiseuille flow over a biphasic mixture (Hou et al. 1989) (dashed lines in Fig. 4a, b). As theoretically predicted, Poiseuille flow had the characteristic parabolic profile in the flow chamber and induced measurable interstitial fluid flow in a boundary layer beneath the TEC hydrogel surface (Fig. 4a). The interstitial fluid velocity at the interface ranged from 26.6 to 65.8 μm/s (Fig. 4b, Table 2). Furthermore, with increasing flow rate, the boundary layer thickness decreased while the flow velocity gradients increased. To better visualize the effects of flow rate on interstitial flow gradients, the fluid velocity in the flow channel and within the hydrogel were normalized by the maximum flow velocity in the channel for each of the flow rates and plotted as a function of depth (Fig. 4c). This plot suggests that the thickness of the interstitial boundary layer was increased at the lower flow rates, implying an increased apparent permeability of the hydrogel. This observation agrees with theory which suggests that the thickness of the boundary layer is influenced by the ratio of
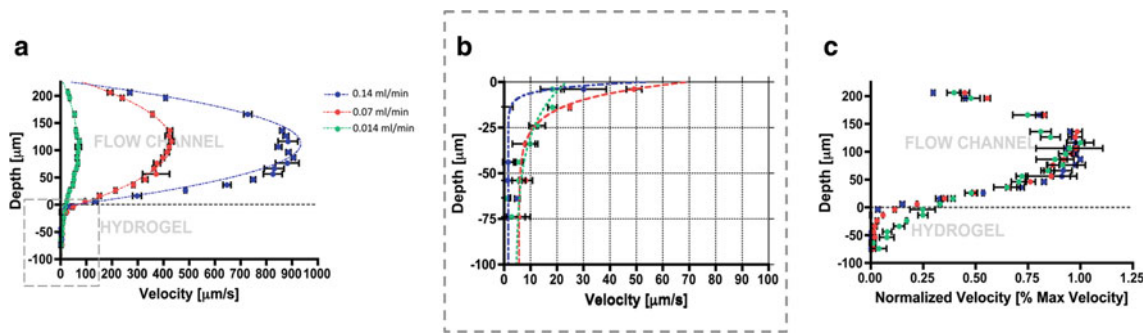
Fig. 4 Flow velocity profiles within the flow chamber and the TEC hydrogels were experimentally measured as a function of flow rate through the scaled-down parallel-plate (Poiseuille flow) bioreactor and fitted to theoretical predictions of Poiseuille flow over a biphasic mixture (Hou et al. 1989). **a** Experimental measurements (symbols, mean ± SEM, $n = 3$ independent experiments per flow rate) and theoretical fits (lines) of the flow velocity profile at pump rates of 0.014, 0.07, and 0.14 ml/min. **b** Depth-dependent interstitial flow velocity gradients within a boundary layer near the flow-exposed surface of the TEC hydrogel. **c** Velocity profiles normalized by the maximum velocity in the flow channel demonstrate that the thickness of the boundary layer with enhanced interstitial flow decreases with increasing flow rate and surface shear stress

Table 2 Interstitial flow parameters determined from fitting the experimentally measured flow velocities to the theoretical biphasic model (Hou et al. 1989)

Poiseuille flow rate (ml/min)	Interfacial flow velocity (μm/s)	Interfacial shear stress ($\times 10^{-3}$ Pa)	Apparent Darcy's permeability (m^2)
0.014	26.59 (5.98)	0.60 (0.117)	3.79×10^{-10} (9.92×10^{-11})
0.07	65.79 (5.26)	3.6 (0.28)	7.13×10^{-11} (1.50×10^{-11})
0.14	42.59 (6.84)	8.2 (0.86)	6.17×10^{-12} (2.52×10^{-12})

Values presented are mean (SEM) of triplicate independent measurements

viscous to drag forces, $\mu_a / K h^2$, where μ_a is the apparent viscosity of the interstitial fluid within the hydrogel, K is the interstitial drag coefficient, and h is the hydrogel thickness (Hou et al. 1989). The drag coefficient was calculated from fitting the experimental data to the theoretical solution (Sect. 1, Supplemental Data), and the apparent Darcian permeability (κ) of the hydrogel was estimated from the drag coefficient using the equation $\kappa = \phi^{f^2} \mu_f / K$, where ϕ^f is the interstitial fluid volume fraction (Hou et al. 1989), which confirmed the qualitative observation of decreased hydrogel permeability with increased flow rate (Table 2).

3.3 Apparent hydrogel permeability decreases exponentially with increased interfacial shear stress

The shear stress profiles in the flow channel and within the hydrogels (Fig. 5a, b) were determined using computational fluid dynamics (CFD) modeling (see Sect. 2 in the supplemental data file) based on the experimentally estimated hydrogel permeability. The interfacial (hydrogel surface) shear stress increased linearly from 0.6×10^{-3} to 8.2×10^{-3} Pa when the flow rate was increased from 0.014 to 0.14 ml/min (Table 2). Interestingly, the interstitial shear stress gradients within the boundary layer also increased with increasing flow rate (Fig. 5b, c). Furthermore, we observed

that in this flow configuration, the increase in interfacial shear stress was associated with an exponential reduction in the apparent permeability of the hydrogel (Fig. 6). Interestingly, the relationship between the apparent permeability and the interfacial shear stress fits an exponential function of the form $k = k_o \times \exp(-M\tau)$, where M is an empirical shear stress-dependent permeability factor (Pa^{-1}).

3.4 Convective mass transport enhancement correlates with interstitial flow gradients

To formally evaluate whether Poiseuille-driven flow improves interstitial mass transport, FRAP-based measurements under flow (0.07 ml/min) or no flow were repeated for different depths within 2% agarose hydrogel slabs saturated in aqueous solutions of various molecular weight FITC-dextran (4, 10, 40, and 70 kDa). Under no-flow conditions where diffusion is the only mode of interstitial fluorescence recovery, there were no depth-dependent effects regardless of the dextran molecular size (dotted black line plots—Fig. 7a–d). Furthermore, quantification of the area under the normalized fluorescence recovery (NFR) curve demonstrated the expected inverse effects of molecular size on the diffusive recovery of fluorescence (black bars in Fig. 7e). On the other hand, Poiseuille flow significantly accelerated fluorescence
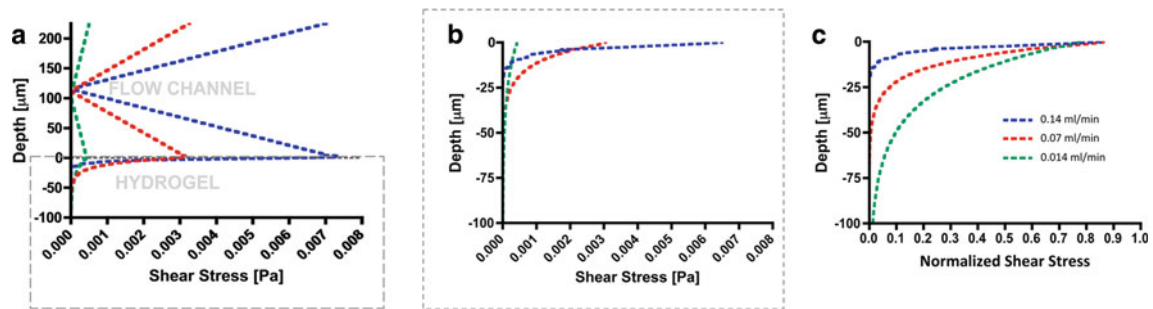
Fig. 5 Poiseuille flow-induced shear stress profiles. **a** Shear stress plots in the parallel-plate bioreactor estimated from computational fluid dynamics (CFD) simulations of the flow using the experimentally estimated apparent permeability values at 0.014, 0.07, and 0.14 ml/min pump flow rates. **b** The interstitial shear stress gradients within the TEC hydrogel. **c** Interstitial shear stress profiles normalized by the shear stress at the hydrogel surface
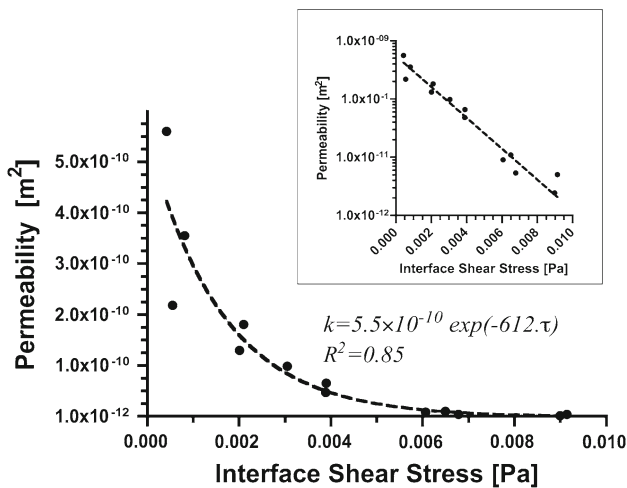

Fig. 6 The apparent permeability of the 2% agarose hydrogel in the parallel-plate bioreactor decreases exponentially with increasing surface shear stress. The flow velocity was measured using FRAP at pump flow rates of 0.014, 0.04, 0.07, 0.1, and 0.14 ml/min in three separate experiments and fitted to the theoretical solution of Poiseuille flow over a biphasic mixture (Hou et al. 1989) to determine the apparent hydrogel permeability, which is then plotted against the shear stress at the hydrogel surface demonstrating the inverse exponential relationship between the apparent Darcian permeability and the fluid-hydrogel interface shear stress (Inset: semi-log scale plot)

recovery near the surface of the hydrogel ($z = 0$) compared with diffusive recovery under no-flow conditions (red line vs. dotted black line plots in Fig. 7a–d), which was confirmed by quantifying the area under the NFR curve (red bars vs. black bars in Fig. 7e), suggesting that convective transport was the dominant mechanism of interstitial fluorescence recovery near the surface regardless of the molecular size. With increasing depth (20 microns) below the hydrogel surface, the convective contribution to fluorescence recovery decreased significantly (blue line plots and bars in Fig. 7). At 50 microns below the surface of the hydrogel, interstitial fluorescence recovery under flow approached the rates

measured for the diffusive no-flow conditions (green line plots in Fig. 7a–d), and was inversely influenced by the molecular size (green bars in Fig. 7e), suggesting that convective flow does not affect interstitial transport at depths ≥ 50 microns.

4 Discussion

Interstitial fluid flow in articular cartilage develops secondarily to compressive and shear deformations during joint articulating motion (Carter et al. 2004). Given its significant influence on cartilage health and disease, it is postulated that interstitial fluid flow has important consequences in cartilage tissue engineering (Guilak et al. 2001; Mow and Wang 1999). The effects of interstitial fluid flow and the flow-induced viscous and drag forces on material inhomogeneity in the porous and permeable ECM of native and engineered cartilage are multifold: First, interstitial fluid flow is thought to transduce frictional drag, streaming potentials, and/or ion transport to effect mechano-electro-chemical intracellular signaling. Second, interstitial fluid flow may improve mass transport via convection of solutes and nutrients to increase the metabolism of chondrocytes in the tissue engineered cartilage. Third, interstitial fluid flow induces frictional drag forces that may directly influence the compaction and alignment of collagen fibers in the ECM (Mow and Wang 1999). Thus, we hypothesized that inducing gradients of interstitial flow through engineered cartilage hydrogel could lead to material and structural inhomogeneities in the ECM. To test this, we designed a hydrodynamic bioreactor chamber that simulates Poiseuille flow over TEC hydrogels (chondrocyte-seeded agarose constructs). Our experimental results demonstrated increased production of type II collagen and glycosaminoglycan in a superficial region of the hydrogel that was in contact with the flow; however, the deeper regions of the hydrogels do not appear to recapitulate the zonal
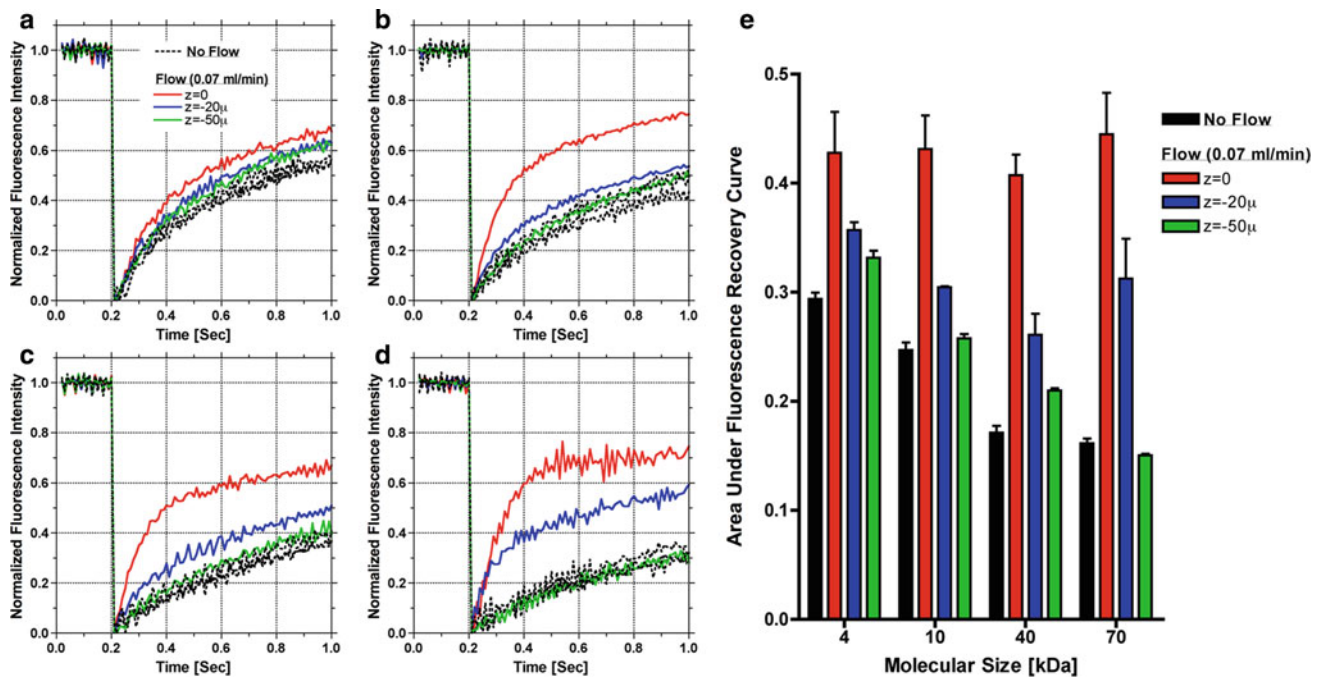
Fig. 7 Assessment of convective and diffusive interstitial transport based on FRAP measurements under Poiseuille flow (0.07 ml/min) or no flow. The normalized fluorescence intensity (NFR) within the *bleached region* is measured at various depths within the 2% agarose hydrogel and plotted versus time for **a** 4 kDa, **b** 10 kDa, **c** 40 kDa, **d** 70 kDa molecular weight FITC-conjugated dextran. **d** The area under the NFR curve was computed to compare the dextran transport rates as a function of hydrogel depth and molecular size. *Black dots* represent individual fluorescence measurements for all depths under no-flow condition. Data presented as mean ±SEM from duplicate measurement in two independent experiments

anisotropic structure of the native tissue, which suggests that other mechanical signals and biological factors might be involved in the native tissue anisotropy. These observations corroborate previous findings by others (Gemmiti and Guldberg 2006, 2009). In these experiments, Gemmiti and Guldberg stimulated engineered cartilage constructs made up of scaffoldless, self-assembled chondrocytes and *de novo* secreted ECM using laminar Poiseuille flow at variable shear stresses ranging from 0 (static) to 0.1 Pa. They demonstrated that flow-induced shear stresses stimulated spatial heterogeneity in the deposition of types I and II collagens in the ECM region exposed to flow and significantly increased the tensile strength and moduli of these thin strips of engineered cartilage constructs. They further reported that increasing the shear stress, while increasing the overall collagen content and tensile strength, also increased the area fraction of type I collagen ECM and fibroblastic-looking cells in the region of the construct exposed to flow (Gemmiti and Guldberg 2009), which suggests a reversion to a fibrocartilage phenotype with increasing shear stress. They concluded based on the reported values of hydraulic permeability of cartilage and their own measurements of their constructs' permeability that these effects are directly related to the shear stress and likely independent of interstitial flux. While there are

many similarities between these studies and our current work, there are also important differences. Gemmiti investigated flow-induced shear effects on thin scaffold-free cartilage constructs (~ 250 microns), while our constructs were composed of thick (~ 2 mm) chondrocyte-seeded agarose hydrogels, which maintain the chondrocytes in a rounded morphology thereby inhibiting their dedifferentiation to a fibroblastic phenotype and their propensity to produce type I collagen (Awad et al. 2004). Furthermore, our constructs were stimulated periodically with oscillating (sinusoidal) flow at nominal shear stress amplitude of ±0.012 Pa, which was within the range but not specifically investigated by Gemmiti, making a direct comparison of the observed effects difficult. More importantly, our agarose hydrogels comprise 98% interstitial water with a nominal hydraulic permeability about 4 orders of magnitude higher than cartilage (Mauck et al. 2000), which we demonstrated to be permissive of interstitial flux under the flow conditions applied herein.

To the best of our knowledge, this is the first report of direct experimental measurements of interstitial fluid flow fields through bioreactor-cultivated engineered cartilage hydrogels. The experimentally determined velocity profiles faithfully fit theoretical predictions previously derived by Hou et al. (1989). The maximum interstitial fluid velocity in the

hydrogel was about 1 to $1\frac{1}{2}$ orders of magnitude higher than the values reported for compression-induced interstitial flow in cartilage (Buschmann et al. 1995; Mow and Wang 1999), which seems intuitively reasonable given the differences in hydraulic permeability between the native tissue and the agarose hydrogel.

Based on the interstitial fluid velocity measurements and the theory, we estimated the apparent hydrogel permeability under the various flow conditions and made the observation that the apparent hydrogel permeability decreases with increasing flow rate and hence shear stress at the hydrogel surface. The permeability of hydrated mixtures such as biological tissues and engineered hydrogels is an intrinsic property that governs interstitial fluid flow and is typically estimated using Darcy's Law, which for a unidirectional flow in a hydrogel column with cross-sectional area (A) predicts that the volumetric flow rate (Q) or the average velocity (v) of a Newtonian fluid through the hydrogel is directly proportional to the pressure drop (ΔP) across the column height (h).

$$v = \frac{Q}{A} = \frac{\kappa}{\mu} \frac{\Delta P}{h} \qquad (8)$$

The proportionality constant is defined as the hydraulic permeability ($k = \kappa/\mu$), which is the ratio of Darcy's permeability of the hydrogel (κ) to the dynamic viscosity of the fluid (μ). The permeability is often reported for native and engineered cartilage as a material property and has significant implications for tissue biomechanics and interstitial transport (diffusion and convection) (Mow and Wang 1999).

We observed that our 2% agarose gel permeability predictions were several orders of magnitude higher than the range of intrinsic permeability values reported in the literature from permeation and confined compression experiments (Gu et al. 2003; Johnson and Deen 1996; Mauck et al. 2000). One potential cause is that our FRAP-based measurements were done in a hyposmotic aqueous solution and could not, due to technical difficulties, be reproducibly performed at physiologic ionic strength that would replicate the culture conditions. However, it has been recently shown that decreasing the ionic strength of negatively-charged agarose-GAG gels by 2 orders of magnitude results in only a two-fold decrease in Darcy's permeability (Mattern et al. 2008). In our electrically neutral agarose hydrogels, the opposite effects might be expected due to the lack of charged species within the gel, although the magnitude of the hypotonic effect is expected to be similarly small, hence suggesting this mechanism is not the reason behind the observed discrepancy in permeability values. On the other hand, it is possible that small reductions in agarose concentration (e.g. increases in the water fraction and porosity) could result in more pronounced permeability increases, compared with

changes in ionic strength, as has been experimentally determined (Gu et al. 2003; Maroudas et al. 1969). However, based on the empirical relationship between hydraulic permeability and the water/solid fraction of the agarose gel described by Gu et al. (2003), the potential inaccuracies in preparing the agarose hydrogel at the nominal concentration are not sufficient to explain the observed discrepancy in the permeability values. The more plausible explanation has in fact been described by Beavers and Joseph (1967) in the context of deriving and experimentally validating the boundary conditions at a permeable construct interface subject to free flow, in which they argued that enforcing conservation of mass and linear momentum of the fluid phase at the interface between the free flow and the agarose hydrogel induces a "*boundary layer*" in the hydrogel within which the interstitial fluid flow velocity departs from Darcian predictions (e.g. significantly higher). Furthermore, within this boundary layer, the velocity changes rapidly from its "slip" value at the interface to the Darcy's value deeper within the hydrogel, giving rise to the observed flow gradients. Thus, the boundary layer phenomenon, which does not conform to Darcy's estimation, results in an increase in the interstitial flow near the hydrogel interface with the free flow in the Poiseuille channel, consequently leading to an increase in the *apparent* permeability of the hydrogel. In other words, strictly using the Darcian permeability values in simulating this problem fails to predict this boundary layer phenomenon and leads to the wrong conclusion that interstitial fluid flow near the interface is negligible.

Moreover, the velocity gradients within the boundary layer appear to be proportional to the shear stresses at the interface, such that the thickness of this interstitial boundary layer decreases with increasing flow rate and interfacial shear stress, which explains the inverse exponential relationship between the interface shear stress and the apparent hydrogel permeability. The original observation that the apparent permeability of the hydrogel decreases exponentially with increasing shear stress at the free fluid-hydrogel interface bears striking similarity to the well-described phenomenon of deformation-dependent permeability under compressive loading, which is empirically modeled as an inverse exponential relationship (Mow et al. 1984). Previous reports corroborate our findings and suggest that the permeability of biological tissues or engineered scaffolds can be an effective indicator of shear stresses in these systems (Vossenberg et al. 2009; Wang and Tarbell 1995). In agreement with our observation, Vossenberg et al. (2009) recently demonstrated using a finite element model that the average and maximum shear stress in perfused printed scaffolds increases significantly with decreased porosity (and hence reduced permeability) and appears insensitive to pore size (Vossenberg et al. 2009). While the permeability data empirically fit an inverse exponential function of the interface shear stress, this curve fit and

the continuum assumption used for predicting the interstitial flow fields and permeability do not explain this phenomenon. Under compression, the reduction in permeability is attributed to reductions in the effective porosity and the pore size, which contributes to fluid pressurization and enables cartilage to support large compressive loads. The mechanism of shear stress-dependent permeability in our system is less clear, but could theoretically arise from compaction of the pores at the interface that effectively reduces their opening size and provides greater resistance to interstitial flow, similar to the mechanism observed under compression. We hypothesize that there exists a flow threshold below which no significant deformations are experienced by the pore walls at the hydrogel surface, and therefore, the interstitial velocity at the interface increases with flow rate, which explains the increased interstitial velocity observed at the intermediate flow rate. When the flow rate increases beyond this threshold, the pore walls at the surface deform substantially and their openings reduce, which explains the reduction in the interstitial fluid velocity at the higher flow rate. This suggests that the interstitial boundary layer flow depends not only on intrinsic material properties such as the permeability but also on the structural nature of the porous interface (Beavers and Joseph 1967).

It should be noted that in scaling the bioreactor to enable the experimental flow measurements, we maintained the ratio of the flow channel height to the biphasic layer thickness $\lambda = h_1/h_2$. We also varied the pump flow rate to maintain the same nominal interfacial shear stress range in the two experiments. Given that the material properties of the hydrogel and fluid are initially the same in the two systems, we believe that the observations from the experimental measurements of interstitial flow are representative of the scaled-up bioreactor used to cultivate the chondrocyte-seeded hydrogels. There are, however, important differences including the fact that flow in the cell culture experiments was oscillatory, while the flow in the FRAP experiments was steady for practical reasons. Furthermore, the accrual of the ECM in the larger chondrocyte-seeded engineered cartilage hydrogel was not accounted for in the scaled-down FRAP bioreactor measurements, which were done in a cell-free 2% agarose hydrogel representing the initial material property of the chondrocyte-seeded hydrogel at day 0. We hypothesize that as new ECM is produced, the permeability of the engineered constructs, and consequently the interstitial fluid flow, would decrease. Formal investigation of this hypothesis will be the subject of future studies.

The inverse nonlinear relationship between the interfacial shear stress and the apparent gel permeability has significant implications for cartilage tissue engineering. While shear stress has important mechanostimulatory consequences for cartilage tissue engineering (Gemmiti and Guldberg 2006, 2009; Pazzano et al. 2000; Saini and Wick 2003; Stoddart et al. 2006), its effects on permeability and consequently on interstitial nutrient transport should not be overlooked. We demonstrated in this experiment that Poiseuille-induced interstitial flow enhances convective transport of FITC-conjugated, neutral dextran molecules in a boundary layer ($\sim$ 50 microns) of high fluid flow near the surface of the hydrogel, independent of molecular size (for the range of 3–70 kDa). These results correlate with interstitial flow measurements, which were negligible at depths $\geq$ 50 microns, approximately the thickness of the boundary layer at a flow rate of 0.07 ml/min (Fig. 4b, c). Theoretically, the thickness of the boundary layer of enhanced flow in the larger "cell culture" bioreactor should scale-up in proportion to the thickness of the hydrogel (Sect. 1, Supplemental Data), which might explain the thicker region (240 microns) of enhanced cell metabolic activity (Fig. 3). Additionally, gradients of soluble factors created as a result of the enhanced transport and mechanostimulation in the boundary layer might lead to paracrine signal effects that extend beyond that layer. The convective transport decreased with depth through the hydrogel in association with the measured interstitial flow gradients, such that at depths where fluid flow was negligible the transport was dominated by passive diffusion. We posit that increasing the interface shear stress at the interface with the hydrogel (by increasing the Poiseuille flow rate) and the associated decrease in apparent hydrogel permeability will hinder convective transport and affect the material inhomogeneity within the engineered TEC hydrogels. This hypothesis warrants formal investigation in future studies, especially since the broader significance of the inverse relationship between the interfacial shear stress on one hand and interstitial permeability and convective transport on the other is not limited to our experimental setup. Indeed, a variety of scaffolds for cartilage tissue engineering comprise interconnected porous channels whose walls are lined with seeded cells and their newly secreted ECM. These porous networks can be approximated as Poiseuille flow channels through which fluid (i.e. culture media) flows past the neotissue lining the pores as a result of dynamic compressive stimulation or direct perfusion. Therefore, striking a balance between the mechanostimulatory effects of the flow-induced shear stress and the potential hindrance of permeability and interstitial convective transport to the neotissue lining the porous scaffold walls should be an important design consideration in tissue engineering bioreactor systems.

References

Awad HA, Wickham MQ, Leddy HA, Gimble JM, Guilak F (2004) Chondrogenic differentiation of adipose-derived adult stem cells in agarose, alginate, and gelatin scaffolds. Biomaterials 25(16): 3211–3222

Beavers GS, Joseph DD (1967) Boundary conditions at a naturally permeable wall. J Fluid Mech 30:197–207

Bonassar LJ, Grodzinsky AJ, Frank EH, Davila SG, Bhaktav NR, Trippel SB (2001) The effect of dynamic compression on the response of articular cartilage to insulin-like growth factor-I. J Orthop Res 19(1):11–17

Bujia J, Sittinger M, Minuth WW, Hammer C, Burmester G, Kastenbauer E (1995) Engineering of cartilage tissue using bioresorbable polymer fleeces and perfusion culture. Acta Otolaryngol 115(2):307–310

Buschmann MD, Gluzband YA, Grodzinsky AJ, Hunziker EB (1995) Mechanical compression modulates matrix biosynthesis in chondrocyte/agarose culture. J Cell Sci 108(Pt 4):1497–1508

Buschmann MD, Kim YJ, Wong M, Frank E, Hunziker EB, Grodzinsky AJ (1999) Stimulation of aggrecan synthesis in cartilage explants by cyclic loading is localized to regions of high interstitial fluid flow. Arch Biochem Biophys 366(1):1–7

Butler DL, Goldstein SA, Guilak F (2000) Functional tissue engineering: the role of biomechanics. J Biomech Eng 122(6):570–575

Carter DR, Beaupre GS, Wong M, Smith RL, Andriacchi TP, Schurman DJ (2004) The mechanobiology of articular cartilage development and degeneration. Clin Orthop Relat Res (427 Suppl): S69–S77

Carter DR, Wong M (2003) Modelling cartilage mechanobiology. Philos Trans R Soc Lond B Biol Sci 358(1437): 1461–1471. doi:10.1098/rstb.2003.1346

Freed LE, Hollander AP, Martin I, Barry JR, Langer R, Vunjak-Novakovic G (1998) Chondrogenesis in a cell-polymer-bioreactor system. Exp Cell Res 240(1):58–65

Freed LE, Vunjak-Novakovic G, Langer R (1993) Cultivation of cell-polymer cartilage implants in bioreactors. J Cell Biochem 51(3):257–264

Gemmiti CV, Guldberg RE (2006) Fluid flow increases type II collagen deposition and tensile mechanical properties in bioreactor-grown tissue-engineered cartilage. Tissue Eng 12(3):469–479

Gemmiti CV, Guldberg RE (2009) Shear stress magnitude and duration modulates matrix composition and tensile mechanical properties in engineered cartilaginous tissue. Biotechnol Bioeng 104(4):809–820

Gray ML, Pizzanelli AM, Grodzinsky AJ, Lee RC (1988) Mechanical and physiochemical determinants of the chondrocyte biosynthetic response. J Orthop Res 6(6):777–792

Gu WY, Yao H, Huang CY, Cheung HS (2003) New insight into deformation-dependent hydraulic permeability of gels and cartilage, and dynamic behavior of agarose gels in confined compression. J Biomech 36(4):593–598

Guilak F, Butler DL, Goldstein SA (2001) Functional tissue engineering: the role of biomechanics in articular cartilage repair. Clin Orthop Relat Res (391 Suppl):S295–S305

Hou JS, Holmes MH, Lai WM, Mow VC (1989) Boundary conditions at the cartilage-synovial fluid interface for joint lubrication and theoretical verifications. J Biomech Eng 111(1):78–87

Hung CT, Mauck RL, Wang CC, Lima EG, Ateshian GA (2004) A paradigm for functional tissue engineering of articular cartilage

via applied physiologic deformational loading. Ann Biomed Eng 32(1):35–49

Johnson EM, Deen WM (1996) Hydraulic permeability of agarose gels. Aiche J 42(5):1220–1224

Lamkin-Kennard KA, King MR, Awad HA (2005) A novel lid-driven cavity flow bioreactor for cartilage tissue engineering. In: Proceedings of the 2005 summer bioengineering conference, Vail, CO, USA. American Society of Mechanical Engineers, pp 1060–1061

Lammi MJ (2004) Current perspectives on cartilage and chondrocyte mechanobiology. Biorheology 41(3–4):593–596

Leddy HA, Haider MA, Guilak F (2006) Diffusional anisotropy in collagenous tissues: fluorescence imaging of continuous point photobleaching. Biophys J 91(1):311–316

Lee HS, Millward-Sadler SJ, Wright MO, Nuki G, Salter DM (2000) Integrin and mechanosensitive ion channel-dependent tyrosine phosphorylation of focal adhesion proteins and beta-catenin in human articular chondrocytes after mechanical stimulation. J Bone Miner Res 15(8):1501–1509

Malone AM, Anderson CT, Tummala P, Kwon RY, Johnston TR, Stearns T, Jacobs CR (2007) Primary cilia mediate mechanosensing in bone cells by a calcium-independent mechanism. Proc Natl Acad Sci USA 104(33):13325–13330

Maroudas A, Muir H, Wingham J (1969) The correlation of fixed negative charge with glycosaminoglycan content of human articular cartilage. Biochim Biophys Acta 177(3):492–500

Mattern KJ, Nakornchai C, Deen WM (2008) Darcy permeability of agarose-glycosaminoglycan gels analyzed using fiber-mixture and donnan models. Biophys J 95(2):648–656

Mauck RL, Soltz MA, Wang CC, Wong DD, Chao PH, Valhmu WB, Hung CT, Ateshian GA (2000) Functional tissue engineering of articular cartilage through dynamic loading of chondrocyte-seeded agarose gels. J Biomech Eng 122(3):252–260

Mauck RL, Wang CC, Oswald ES, Ateshian GA, Hung CT (2003) The role of cell seeding density and nutrient supply for articular cartilage tissue engineering with deformational loading. Osteoarthr Cartil 11(12):879–890

Mow VC, Wang CC (1999) Some bioengineering considerations for tissue engineering of articular cartilage. Clin Orthop Relat Res (367 Suppl):S204–S223

Mow VC, Holmes MH, Lai WM (1984) Fluid transport and mechanical properties of articular cartilage: a review. J Biomech 17(5):377–394

Pazzano D, Mercier KA, Moran JM, Fong SS, DiBiasio DD, Rulfs JX, Kohles SS, Bonassar LJ (2000) Comparison of chondrogensis in static and perfused bioreactor culture. Biotechnol Prog 16(5):893–896

Pierre J, Gemmiti CV, Kolambkar YM, Oddou C, Guldberg RE (2008) Theoretical analysis of engineered cartilage oxygenation: influence of construct thickness and media flow rate. Biomech Model Mechanobiol 7(6):497–510

Polianin AD (2002) Handbook of linear partial differential equations for engineers and scientists. Chapman & Hall/CRC, Boca Raton

Rutkowski JM, Swartz MA (2007) A driving force for change: interstitial flow as a morphoregulator. Trends Cell Biol 17(1): 44–50

Sah RL, Kim YJ, Doong JY, Grodzinsky AJ, Plaas AH, Sandy JD (1989) Biosynthetic response of cartilage explants to dynamic compression. J Orthop Res 7(5):619–636

Saini S, Wick TM (2003) Concentric cylinder bioreactor for production of tissue engineered cartilage: effect of seeding density and hydrodynamic loading on construct development. Biotechnol Prog 19(2):510–521

Shi ZD, Wang H, Tarbell JM (2011) Heparan sulfate proteoglycans mediate interstitial flow mechanotransduction regulating MMP-13

expression and cell motility via FAK-ERK in 3D collagen. PloS one 6(1):e15956

Shieh AC, Swartz MA (2011) Regulation of tumor invasion by interstitial fluid flow. Phys Biol 8(1):015012

Sittinger M, Bujia J, Minuth WW, Hammer C, Burmester GR (1994) Engineering of cartilage tissue using bioresorbable polymer carriers in perfusion culture. Biomaterials 15(6):451–456

Stoddart MJ, Ettinger L, Hauselmann HJ (2006) Enhanced matrix synthesis in de novo, scaffold free cartilage-like tissue subjected to compression and shear. Biotechnol Bioeng 95(6):1043–1051

Vossenberg P, Higuera GA, van Straten G, van Blitterswijk CA, van Boxtel AJ (2009) Darcian permeability constant as indicator for shear stresses in regular scaffold systems for tissue engineering. Biomech Model Mechanobiol 8(6):499–507

Wang DM, Tarbell JM (1995) Modeling interstitial flow in an artery wall allows estimation of wall shear stress on smooth muscle cells. J Biomech Eng 117(3):358–363

Wong M, Carter DR (2003) Articular cartilage functional histomorphology and mechanobiology: a research perspective. Bone 33(1):1–13